Doucet, L.S., et al., 2020, Archean lithospheric differentiation: Insights from Fe and Zn isotopes: Geology, v. 48, https://doi.org/10.1130/G47647.1

Archean lithospheric differentiation: Insights from Fe and Zn isotopes

Luc S. Doucet[1,2], Oscar Laurent[3], Dmitri A. Ionov[4], Nadine Mattielli[1], Vinciane Debaille[1], Wendy Debouge[1]

[1] Laboratoire G-Time, Université Libre de Bruxelles, ULB, CP 160/02, Av. FD Roosevelt, 50, Brussels 1050, Belgium

[2] Earth Geodynamic Research Group, TiGER, Department of Applied Geology, Curtin University, Perth WA 6845, Australia; Corresponding author
luc.serge.doucet@curtin.edu.au.com, tel: +61 (0) 8 92 66 71 07

[3]Institute for Geochemistry and Petrology, ETH Zürich, Claussiusstrasse 25, 8038, Switzerland

[4]Geoscience Montpellier, Université de Montpellier, 34095, Montpellier, France

SUPPLEMENTARY DATA

Analytical methods

Iron purification

The entire acid dissolution procedure and the Fe chromatographic purification were achieved under class-100 flow hood in a class- 1000 clean lab at Laboratoire G-Time at Université Libre de Bruxelles (ULB). For the quality of the reagents, see details in (Doucet et al., 2016). The powders (~5-10 mg) were successively dissolved in 5 ml concentrated HF-HNO3 mix (3:2), HCl-HNO3 (1:1) and HCl. Fe was purified from the matrix using ion exchange resin AG1-X8 100-200 mesh. The column yields are 99±0.5‰. The total procedural blank gave an average value of 1500ng.

The iron isotope compositions of bulk- rocks were obtained using the sample standard bracketing at Université Libre de Bruxelles (ULB), Belgium on Nu Plasma II (Nu instrument) multi-collector ICP-MS in dry mode using Aridus II for the continental crust samples and at University of British Columbia on Nu 1700 (Nu instrument) multi-collector ICP-MS in dry mode using DSN for the lithospheric mantle samples.

For Nu Plasma II MC-ICP-MS analysis, a 1000pb JMC in-house Ni "dopant" was added to every sample and Fe standards to allow instrumental mass fractionation correction while no "dopant" was used for Nu 1700 MC-ICP-MS analysis. The isotopic data are presented as delta notation relative to the IRMM-14 Fe standard solution. During data acquisition, repeated measurements of IRMM-14 Fe standard solution gave an average value of $\delta^{56}Fe = +0.00 \pm 0.02‰$(2SD) for both Nu Plasma II and Nu 1700 MC-ICP-MS analysis (n>1000). Sample internal precision on $^{56}Fe/^{54}Fe$ and $^{57}Fe/^{54}Fe$ varied from 5 to 6 x 10-6. The reported Fe isotopic compositions for the samples are an average value of at least three 3 replicate analyses and the two-standard deviation (2SD) for each average value range from ±0.01 to ±0.04.

For consistency, the same solution of reference material BHVO-2, BCR-2, G2, GSP-2 and UBN were measured on both instruments (TABLE DR1). In details, BHVO-2 values obtained at ULB and nUBC are similar within the error with $\delta^{56}Fe = +0.10 \pm 0.05‰$ and $+0.06 \pm 0.05‰$ respectively in agreement with the literature (average of literature value with $\delta^{56}Fe = +0.11 \pm 0.03‰$). BCR-2 values at ULB and nUBC are similar within the error with $\delta^{56}Fe = +0.04 \pm 0.05‰$ and $+0.02 \pm 0.05‰$ respectively in general agreement with the literature (average of literature value with $\delta^{56}Fe = +0.09 \pm 0.02‰$). G2 values at ULB and nUBC are similar within the error with $\delta^{56}Fe = +0.21 \pm 0.08‰$ and $+0.32 \pm 0.05‰$ respectively and are within the error with previously published data (+0.13±12‰ and 0.12±0.17‰). Note that the published values for G2 have 2SD error exceeding 0.1‰. GSP-2 values at ULB and nUBC are similar within the error with $\delta^{56}Fe = +0.18 \pm 0.06‰$ and $+0.16 \pm 0.01‰$ respectively, and are in good agreement with published data (average of literature value with $\delta^{56}Fe = +0.16 \pm 0.01‰$). UBN values at ULB and nUBC are similar within the error with $\delta^{56}Fe = +0.06 \pm 0.04‰$ and $+0.03 \pm 0.02‰$ respectively and are in good agreement with published data (average of literature value with $\delta^{56}Fe = +0.05 \pm 0.04‰$). Based on these results, we can have confidence in the external reproducibility of the two instruments to be similar to other available published studies for the same reference material (TABLE DR1). Because internal standard deviation of the 3 replicates obtained during analyses do not reflect the external reproducibility between ULB and UBC we decided to assign a general uncertainty to the average Fe isotopic compositions of each sample analyzed in this study equivalent to ±0.05% which correspond to the average uncertainties (2SD) on the reference material obtained at ULB and nUBC. This general uncertainty of +0.05% is higher than internal 2SD but avoid over interpretations (Doucet et al., 2018).

TABLE A1. GEOSTANDARD VALUES

N°S	sample	δ^{56}Fe	±	reference
BHVO-2	basalt	**0.10**	**0.05**	this study, ULB
		0.06	**0.05**	this study, nUBC
		0.11	0.03	Craddock and Duphas (2011)
		0.10	0.03	Craddock et al (2013)
		0.13	0.02	Millet et al. (2012)
		0.08	0.03	Xia et al (2017)
		0.11	0.04	Zhao et al (2012)
		0.12	0.05	Telus et al (2012)
		0.12	0.05	Liu et al (2014)
		0.11	0.02	He et al (2014)
		0.11	0.01	Zhao et al (2015)
		0.10	0.03	McCoy-West et al 2018
BCR-2	basalt	**0.04**	**0.05**	this study, ULB
		0.02	**0.05**	this study, nUBC
		0.10	0.03	Millet et al. (2012)
		0.09	0.03	Craddock and Duphas (2011)
		0.07	0.06	Zhao et al (2012)
		0.08	0.08	He et al (2014)
		0.09	0.02	Zhao et al (2015)
G2	granite	**0.21**	**0.08**	this study, ULB
		0.32	**0.05**	this study, nUBC
		0.13	0.12	Chapman et al (2009)
		0.12	0.17	Fehr et al (2008)
GSP-2	granodiorite	**0.18**	**0.06**	this study, ULB
		0.16	**0.01**	this study, nUBC
		0.16	0.04	Craddock and Dauphas (2011)
		0.16	0.06	Liu et al (2014)
		0.15	0.01	He et al (2014)
DTS-2b	dunite	**0.02**	**0.02**	this study, ULB
		0.02	0.04	Dauphas et al (2004)
		0.03	0.01	Craddock and Dauphas (2011)
		0.02	0.06	Craddock et al (2013)
		0.04	0.02	Zhao et al (2015)
UBN	peridotite	**0.04**	**0.04**	this study, ULB
		0.03	**0.02**	this study, nUBC
		0.06	0.01	Craddock and Dauphas (2011)
		0.03	0.03	Poitrasson et al (2013)
		0.06	0.03	Craddock et al (2013)

Zinc purification

The Zn isotope data for the mantle and continental rocks were published in Doucet et al. (2016) and (Doucet et al., 2018) respectively. All the method and results can be found in details in these study.

The sample powders were successively dissolved in 5 ml of a concentrated HF-HNO3 mix (3:2), HCl-HNO3 (1:1) and HCl. Zn was purified from the matrix using ion exchange resin AG1-X8 100-200 mesh. The column yields are 99.0±0.5%. Zinc isotope compositions of bulk rocks were obtained using the sample standard bracketing at Université Libre de Bruxelles, Belgium, using a High Resolution Nu Plasma II (Nu Instruments) multi-collector ICP-MS (MC-ICP-MS) in wet plasma mode. The total procedural blank for stable isotopes was measured on the MC-ICPMS and gave an average value of 10 ng Zn. To correct for possible isobaric interferences from ^{64}Ni on ^{64}Zn, ^{62}Ni was monitored throughout. Ion beam intensities for ^{62}Ni were always lower than 0.01 mV while the total Zn ion beam was more than 6 V. Prior to each MC-ICP-MS session, the dried Zn elution fractions were dissolved in100 µl of concentrated HNO3 before being dissolved in 0.05 M HNO3 and diluted to 300 ppb solution. A 300 ppb JMC in-house Cu "dopant" solution was added to every sample and Zn standards to allow for instrumental mass fractionation correction. Our JMC in-house Zn and Cu standard solutions were calibrated against the JMC-Lyon-03-0749l Zn and NIST SRM 976 Cu reference standards (see Petit et al., 2008).

The isotopic data are presented as delta notation relative to the JMC-Lyon-03-0749l Zn standard solution. The instrumental mass bias was monitored by plotting ln(^{65}Cu/^{63}Cu) versus ln(^{66}Zn/^{64}Zn) values for the in-house standards; in addition, δXZn were converted into delta unit per atomic mass unit (amu) to assess mass-dependent isotopic variation. Details of the correction technique and the global methodology are given in Petit et al. (2008) and Mattielli et al. (2009). During data acquisition, repeated measurements of the in-house Zn(Cu) standard solution gave an average value of δ^{66}Zn = +0.00±0.02‰ (2SD) (n~ 350). Sample internal precisions on the ^{66}Zn/^{64}Zn, ^{67}Zn/^{64}Zn and ^{68}Zn/^{64}Zn varied from 5 to 6x10^{-6}. The reported Zn isotopic compositions for the samples are the average value of at least 3 replicate analyses and the two standard deviations (2SD) for each average value range from ±0.01 to 0.03‰. Repeated analyses of JMC-Lyon-03-0749l gave δ^{66}Zn = +0.11± 0.03‰ (2SD) and δ^{68}Zn = +0.20± 0.05‰ relative to our in-house JMC Zn standard. In order to compare our results with published Zn isotope data we "normalized" our results to the value obtained in our laboratory for JMC-Lyon-03-0749l standard as follows: δ^{66}Znsample = δ^{66}Znraw sample - δ^{66}ZnJMC-Lyon-03-0749l. (cf. calculations proposed by Hoefs (2008)). All Zn isotope compositions are reported relative to this normalization hereon, and following sample-standard bracketing correction.

To evaluate the long-term (months) external reproducibility and accuracy of the Zn isotopic results, we repeatedly measured the certified artificial Zn IRMM-3702 standard solution (Ponzevera et al., 2006) in each run as well as full digestion duplicates of the reference materials BHVO-2 and MUH-1. In addition, we had a full digestion replicate of one peridotite (sample 4500-8). The long-term external reproducibility (2SD) for all these is better than ±0.04‰: ±0.02‰ for IRMM-3702 (n=24), ±0.02‰ for BHVO-2 (n=12) and MUH-1 (n=12), and ±0.04‰ for the peridotite sample 4500-8 (n=12) (Table 1)(Fig.1 of online annex 2). We can have confidence in the accuracy of our Zn isotopic measurements as our results for the artificial and natural reference material solutions are identical to the values reported in the study of Wang et al. (2017), and to available published values for IRMM-3702 (Cloquet et al., 2006; Moeller et al., 2012; Moynier et al., 2017; Petit et al., 2008; Sossi et al., 2015; Wang et al., 2017) and BHVO-2 (Chen et al., 2013; Herzog et al., 2009; Moeller et al., 2012; Moynier et al., 2010; Moynier et al., 2007; Sossi et al., 2015; Telus et al., 2012; Wang et al., 2017). We also measured silica-rich reference material G2 (granite; δ^{66}Zn=+0.36±0.02‰ and +0.37±0.02‰) and GSP-2 (granodiorite; two total duplicates δ^{66}Zn=1.03±0.04‰ and 1.08±0.02‰) as well as total duplicates of samples MAS-24 (granite; δ^{66}Zn=0.44±0.03‰ and +0.47±0.04‰) and SAK-5 (pyroxenite; δ^{66}Zn=+0.09±0.02‰ and +0.09±0.02‰), which again showed a reproducibility range of ±0.04‰. of the external reproducibility at ULB, we decided to assign a general uncertainty to the average Zn isotopic composition of each sample

analyzed in this study equivalent to the maximum external reproducibility on $\delta^{66}Zn$, i.e. ±0.04‰.

REFERENCES CITED

Chen, H., Savage, P.S., Teng, F.-Z., Helz, R.T., Moynier, F., 2013. Zinc isotope fractionation during magmatic differentiation and the isotopic composition of the bulk Earth. Earth and Planetary Science Letters, 369–370(0): 34-42.

Cloquet, C., Carignan, J., Libourel, G., 2006. Isotopic composition of Zn and Pb atmospheric depositions in an urban/periurban area of nothereastern France. Environmental Science Technics, 40(6594-6600).

Doucet, L.S., Laurent, O., Mattielli, N., Debouge, W., 2018. Zn isotope heterogeneity in the continental lithosphere: New evidence from Archean granitoids of the northern Kaapvaal craton, South Africa. Chemical Geology, 476: 260-271.

Doucet, L.S., Mattielli, N., Ionov, D.A., Debouge, W., Golovin, A.V., 2016. Zn isotopic heterogeneity in the mantle: A melting control? Earth and Planetary Science Letters, 451: 232-240.

Herzog, G.F., Moynier, F., Albarède, F., Berezhnoy, A.A., 2009. Isotopic and elemental abundances of copper and zinc in lunar samples, Zagami, Pele's hairs, and a terrestrial basalt. Geochimica et Cosmochimica Acta, 73(19): 5884-5904.

Hoefs, J., 2008. Stable isotope chemistry. Springer, Berlin.

Mattielli, N. et al., 2009. Zn isotope study of atmospheric emissions and dry depositions within a 5 km radius of a Pb–Zn refinery. Atmospheric Environment, 43(6): 1265-1272.

Moeller, K., Schoenberg, R., Pedersen, R.-B., Weiss, D., Dong, S., 2012. Calibration of the New Certified Reference Materials ERM-AE633 and ERM-AE647 for Copper and IRMM-3702 for Zinc Isotope Amount Ratio Determinations. Geostandards and Geoanalytical Research, 36(2): 177-199.

Moynier, F. et al., 2010. Volatilization induced by impacts recorded in Zn isotope composition of ureilites. Chem. Geol., 276(3–4): 374-379.

Moynier, F., Blichert-Toft, J., Telouk, P., Luck, J.-M., Albarède, F., 2007. Comparative stable isotope geochemistry of Ni, Cu, Zn, and Fe in chondrites and iron meteorites. Geochimica et Cosmochimica Acta, 71(17): 4365-4379.

Moynier, F., Vance, D., Fujii, T., Savage, P., 2017. The Isotope Geochemistry of Zinc and Copper. Reviews in Mineralogy and Geochemistry, 82(1): 543-600.

Petit, J.C.J., De Jong, J., Chou, L., Mattielli, N., 2008. Development of Cu and Zn Isotope MC-ICP-MS Measurements: Application to Suspended Particulate Matter and Sediments from the Scheldt Estuary. Geostandards and Geoanalytical Research, 32(2): 149-166.

Ponzevera, E. et al., 2006. Mass Discrimination During MC-ICPMS Isotopic Ratio Measurements: Investigation by Means of Synthetic Isotopic Mixtures (IRMM-007 Series) and Application to the Calibration of Natural-Like Zinc Materials (Including IRMM-3702 and IRMM-651). Journal of the American Society for Mass Spectrometry, 17(10): 1413-1428.

Sossi, P.A., Halverson, G.P., Nebel, O., Eggins, S.M., 2015. Combined Separation of Cu, Fe and Zn from Rock Matrices and Improved Analytical Protocols for Stable Isotope Determination. Geostandards and Geoanalytical Research, 39(2): 129-149.

Telus, M. et al., 2012. Iron, zinc, magnesium and uranium isotopic fractionation during continental crust differentiation: The tale from migmatites, granitoids, and pegmatites. Geochimica et Cosmochimica Acta, 97(0): 247-265.

Wang, Z.-Z. et al., 2017. Zinc isotope fractionation during mantle melting and constraints on the Zn isotope composition of Earth's upper mantle. Geochimica et Cosmochimica Acta, 198: 151-167.

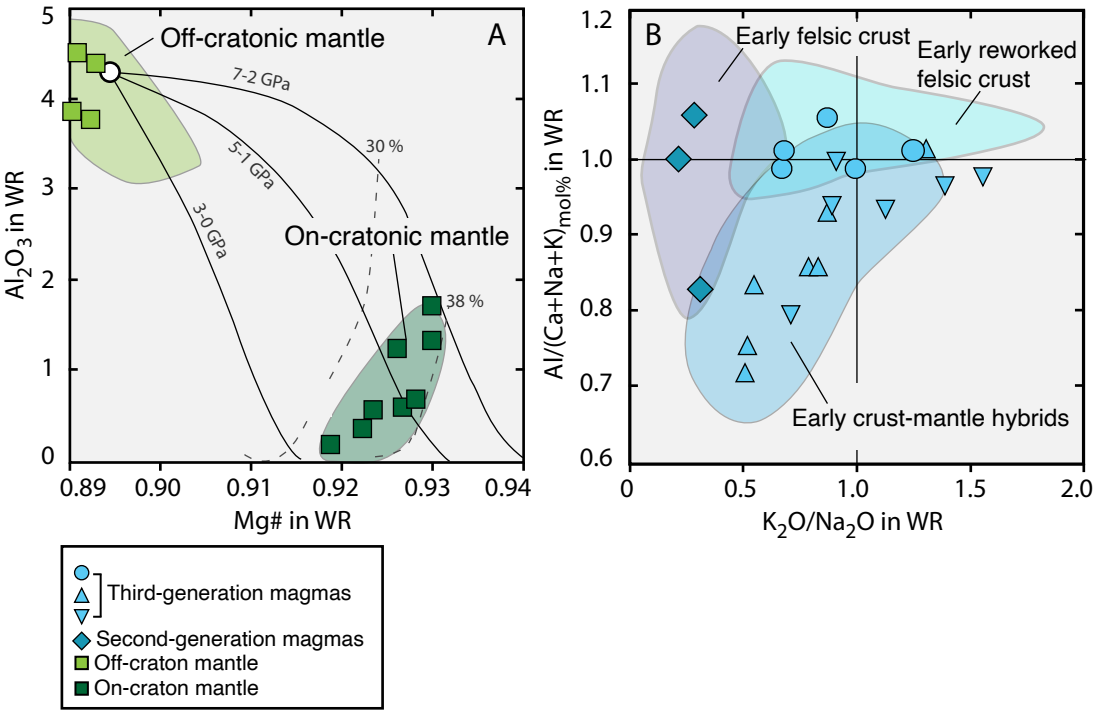

Figure S1. Bulk-rock co-variation diagrams for major elements in mantle peridotites (A) and continental crust rocks (B) in this study compared to the mantle and crustal rock groups they represent. (A) Al_2O_3 vs Mg#([MgO/(MgO+FeOt)])wt% (Doucet et al., 2016; Ionov and Hofmann, 2007) and (B) Bulk rock K_2O/Na_2O vs. molar Al/(-Ca+Na+K) ratio (Laurent et al 2014). Also shown in (A) are experimental melting residues for polybaric fractional melting at 3–0, 5–1 and 7–2 GPa (Doucet et al., 2016; Ionov and Hofmann, 2007).

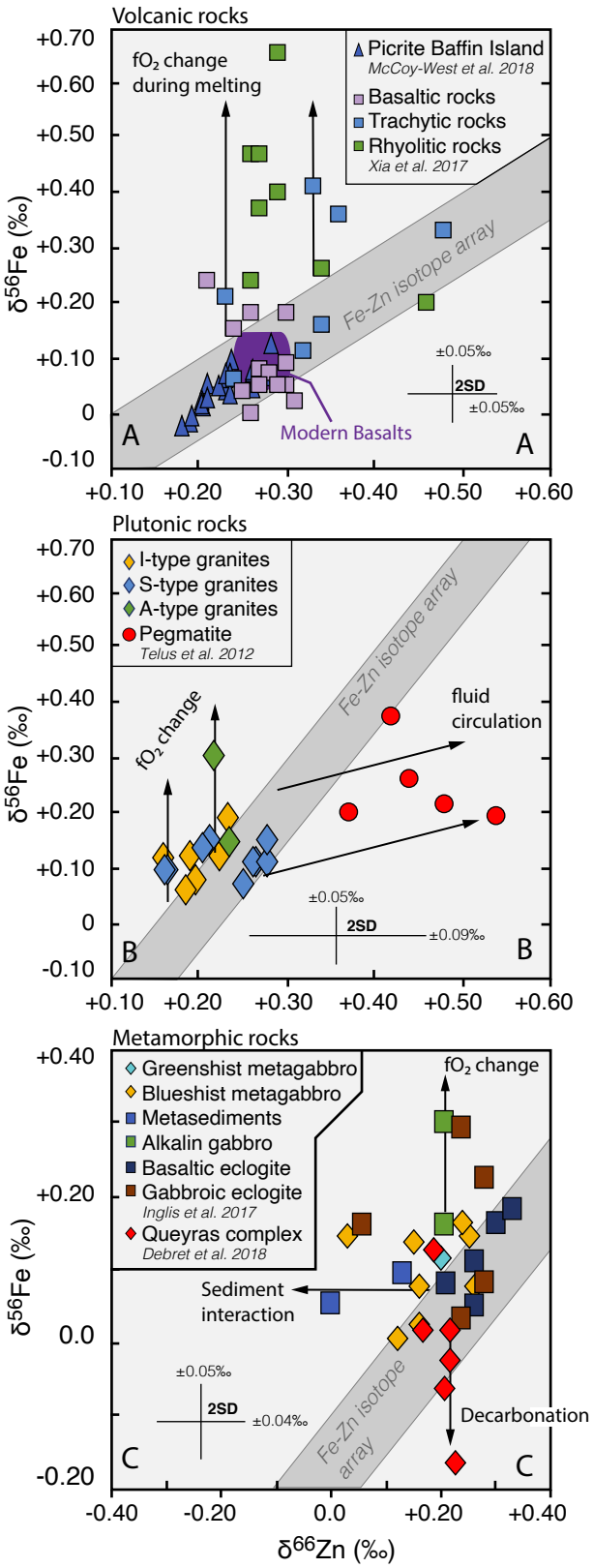

Figure S2. Bulk-rock co-variation diagrams for δ^{56}Fe and δ^{66}Zn in Phanerozoic igneous rocks. (A) Volcanic (Chen et al., 2013; McCoy-West et al., 2018; Xia et al., 2017), (B) plutonic (Telus et al., 2012) and (C) metamorphic (Debret et al., 2018; Inglis et al., 2017) rocks from subduction settings. Arrows illustrate processes invoked by previous studies to explain δ^{56}Fe and/or δ^{66}Zn fractionation: redox change during melting, fluid circulation, interaction with sediments and decarbonation. Also shown are the Fe-Zn isotope array define by the cratonic rocks.

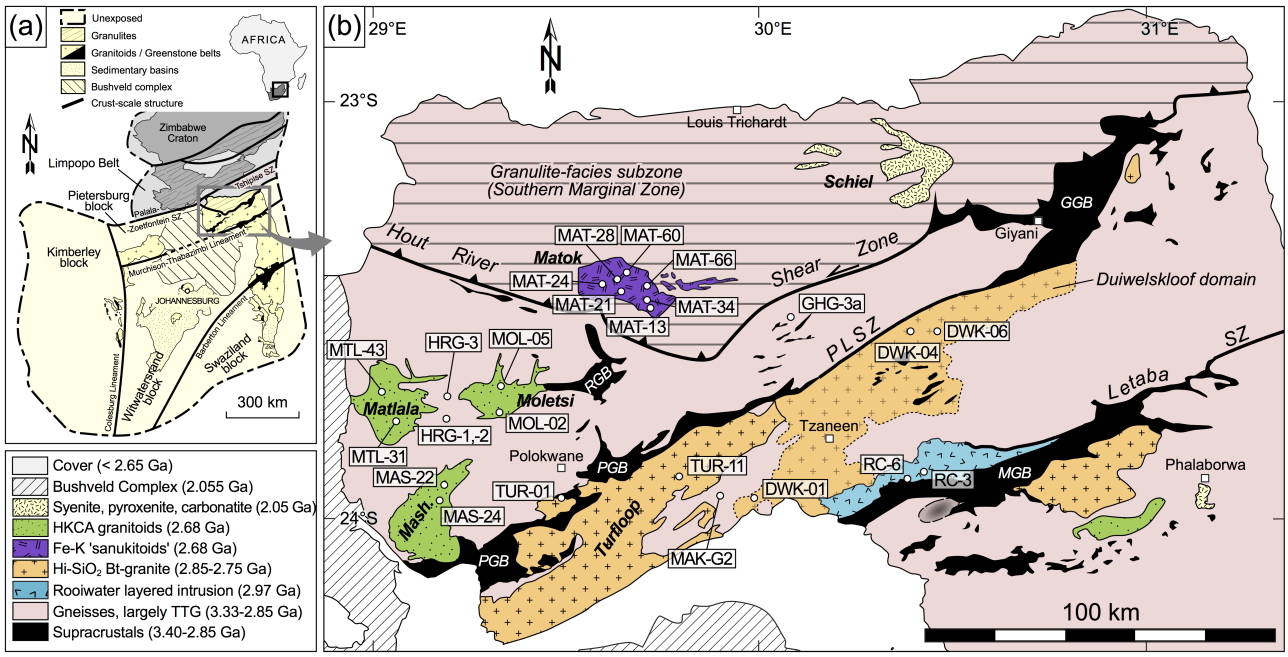

Figure S3. Location map of the samples of samples from the Kaapvaal craton. Schematic structural map highlighting the position of the different crustal domains of the Kaapvaal craton of Southern Africa (after Eglington and Armstrong, 2004); (b) sketch geological map of the Pietersburg block (after Laurent et al., 2013); the age and nature of granitoid rocks are represented by colours and symbols, respectively (granitoid nature according to the classification of Laurent et al., 2014). Labelled spots arelocations of the samples investigated in this study. The ENE–WSW-trendingLetaba, Pietersburg–Lwaji (PLSZ) and Hout River shear zones separate fourdistinct crustal units labelled A to D (see text for details). GGB = Giyani greenstone belt; MGB = Murchison greenstone belt; PGB = Pietersburg, greenstone belt; RGB = Rheno terkoppies greenstone belt. The GPS coordinates are provided in Table 1.

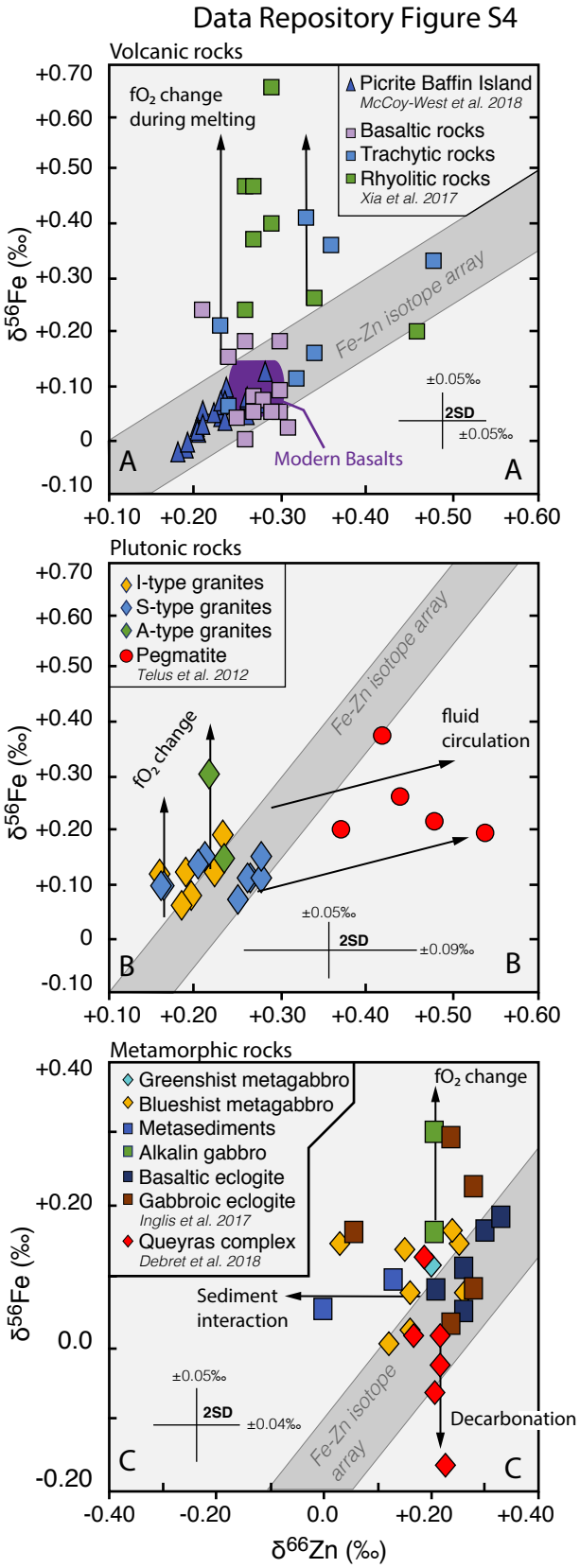

Data Repository Figure S4. Bulk-rock co-variation diagrams for $\delta^{56}Fe$ and $\delta^{66}Zn$ in Phanerozoic igneous rocks. (A) Volcanic (Chen et al., 2013; McCoy-West et al., 2018; Xia et al., 2017), (B) plutonic (Telus et al., 2012) and (C) metamorphic (Debret et al., 2018; Inglis et al., 2017) rocks from subduction settings. Arrows illustrate processes invoked by previous studies to explain $\delta^{56}Fe$ and/or $\delta^{66}Zn$ fractionation: redox change during melting, fluid circulation, interaction with sediments and decarbonation. Also shown are the Fe-Zn isotope array define by the cratonic rocks.

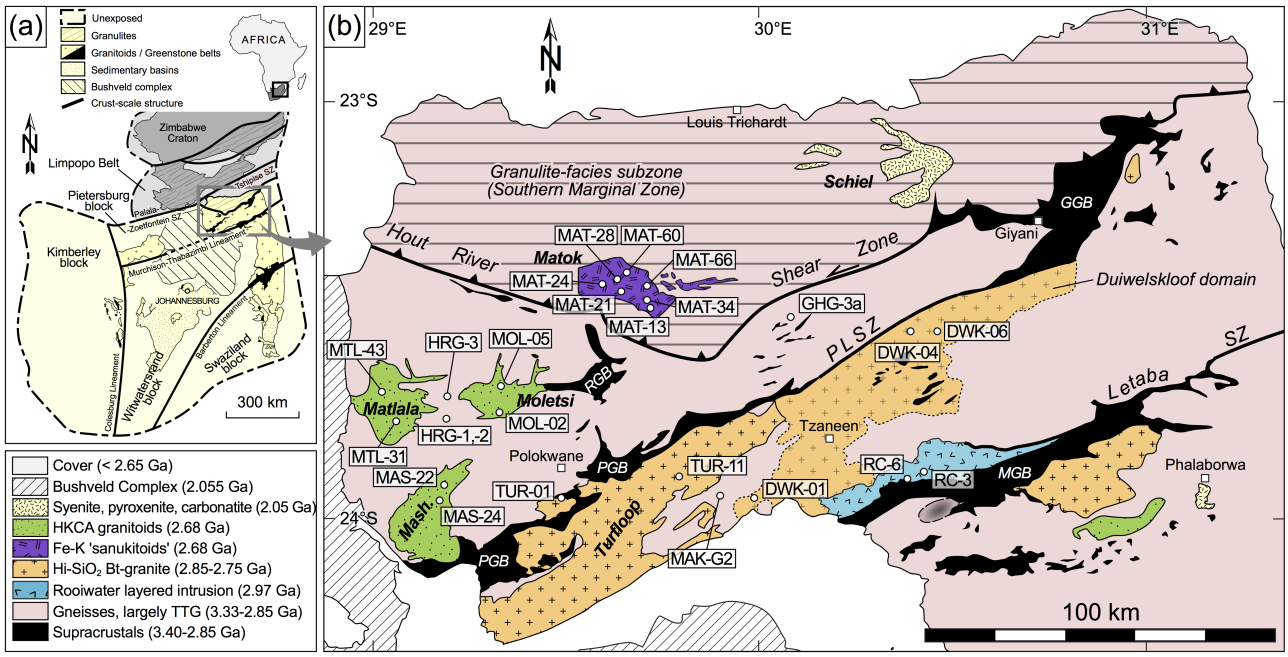

Data Repository Figure S5. Location map of the samples of samples from the Kaapvaal craton. Schematic structural map highlighting the position of the different crustal domains of the Kaapvaal craton of Southern Africa (after Eglington and Armstrong, 2004); (b) sketch geological map of the Pietersburg block (after Laurent et al., 2013); the age and nature of granitoid rocks are represented by colours and symbols, respectively (granitoid nature according to the classification of Laurent et al., 2014). Labelled spots arelocations of the samples investigated in this study. The ENE–WSW-trendingLetaba, Pietersburg–Lwaji (PLSZ) and Hout River shear zones separate fourdistinct crustal units labelled A to D (see text for details). GGB = Giyani greenstone belt; MGB = Murchison greenstone belt; PGB = Pietersburg, greenstone belt; RGB = Rheno terkoppies greenstone belt. The GPS coordinates are provided in Table 1.

Table S1: Fe and Zn isotope data of Pietersburg granitoids in this study compared to U-Pb, Hf and bulk-rock geochemical data

N°S	Rock type	Age	Tectonic	Isotopic data										Bulk-rock geochemical data												
		Ga	stage	εNd(t)	±2SD	εHf(t)	±2SD	δ^{66}Zn	±2SD	δ^{56}Fe	±2SD	δ^{57}Fe	±2SD	SiO_2	TiO_2	Al_2O_3	FeOt	MnO	MgO	CaO	Na_2O	K_2O	P_2O_5	Zn	L.O.I	Sum	Mg#
First-generation magmas																											
Mafic layered intrusion																											
RC-6	Tonalite	2.97	Stage II	n.a.	-	5.10	1.2	0.26	0.04	0.17	0.05	0.32	0.07	69.9	0.83	10.8	9.45	0.13	0.42	3.5	3.7	0.17	0.22	44	0.23	99.3	0.07
RC-3	Gabbro	2.97	Stage II	n.a.	-		-	0.31	0.04	0.09	0.05	0.12	0.07	51.9	0.51	21.2	6.4	0.10	5.2	12	2.8	0.06	0.06	47	1.3	100.2	0.59
								0.29	0.04	0.13	0.06	0.22	0.14														
Second-generation magmas																											
TTG																											
GHG-3a	Diorite	3.34	Stage I	n.a.	-	0.00	1.3	0.30	0.04	0.13	0.05	0.21	0.07	60.3	0.92	16.7	6.2	0.09	3.6	6.2	4.4	1.4	0.21	70	0.43	100.1	0.51
MAK-G2	Trondhjemite	2.95	Stage II	n.a.	-	2.90	1.4	0.31	0.04	0.17	0.05	0.23	0.07	71.7	0.21	15.5	1.5	0.03	0.46	2.1	6.2	1.5	0.09	50	0.22	99.7	0.35
HRG-1	Trondhjemite	2.95	Stage II	0.8	0.9	2.60	1.3	0.45	0.04	0.25	0.05	0.37	0.07	71.9	0.25	15.4	1.3	0.02	0.60	2.9	5.4	1.0	0.12	25	0.77	100.7	0.46
DWK-04	Trondhjemite	2.94	Stage II	0.8	0.9	2.50	0.7	0.42	0.04	0.22	0.05	0.30	0.07	70.7	0.23	15.7	1.3	0.02	0.54	2.4	6.3	1.1	0.10	51	0.32	101.7	0.42
TUR-01	Granite	2.78	Stage III	n.a.	-	-0.40	1.8	0.31	0.04	0.21	0.05	0.33	0.07	71.5	0.22	15.2	1.3	0.02	0.50	2.0	5.4	1.6	0.10	22	1.62	99.8	0.40
Third-generation magmas																											
K-rich granites																											
DWK-06	Granite	2.78	Stage III	-1.2	0.8	0.30	1.7	0.46	0.04	0.22	0.05	0.30	0.07	73.4	0.15	13.7	0.9	0.02	0.29	1.1	4.8	3.3	0.05	30	1.2	99.0	0.36
HRG-2	Leucogranite	2.83	Stage III	-0.4	0.8	2.00	1.2	0.42	0.04	0.23	0.05	0.31	0.07	74.5	0.12	13.5	1.1	0.01	0.17	0.82	3.9	4.9	0.04	28	0.43	99.7	0.23
DWK-01	Granite	2.84	Stage III	-0.9	0.8	0.60	0.9	0.42	0.04	0.20	0.05	0.31	0.07	70.3	0.36	14.8	1.7	0.02	0.57	1.7	4.4	4.3	0.12	38	0.75	99.4	0.37
LET-G2	Leucogranite	2.78	Stage III	n.a.	-	-0.10	2.1	0.45	0.04	0.24	0.05	0.38	0.07	70.9	0.25	15.5	1.7	0.02	0.78	2.1	5.0	3.3	0.15	28	0.56	100.6	0.45
TUR-11	Granite	2.77	Stage III					0.43	0.04	0.22	0.05	0.34	0.07	74.4	0.19	13.8	1.0	0.02	0.33	1.2	4.2	3.6	0.05		0.45	99.5	0.36
Sanukitoids																											
MAT-28	Diorite	2.68	Stage IV	-3.8	0.8		-	0.28	0.04	0.10	0.05	0.19	0.07	57.3	2.0	13.6	9.0	0.12	3.5	6.3	3.4	1.8	0.99	120	0.5	99.4	0.41
MAT-60	Diorite	2.68	Stage IV	-3.3	0.8	-3.60	1.1	0.31	0.04	0.09	0.05	0.10	0.07	59.2	1.5	14.5	7.2	0.11	3.2	5.9	3.8	2.0	0.64	93	0.8	99.7	0.44
MAT-66	Diorite	2.68	Stage IV	-3.4	0.8		-	0.36	0.04	0.12	0.05	0.16	0.07	60.6	1.8	13.9	8.3	0.12	1.9	4.1	4.1	2.3	0.61		1.0	99.5	0.29
MAT-13	Granodiorite	2.68	Stage IV	-2.8	0.8	-3.20	1.1	0.35	0.04	0.13	0.05	0.17	0.07	63.4	1.1	14.5	5.4	0.08	2.2	3.9	3.9	3.2	0.49	64	1.0	99.6	0.41
MAT-21b	Granodiorite	2.68	Stage IV	-3.5	0.8		-	0.34	0.04	0.17	0.05	0.23	0.07	65.2	1.2	13.9	5.2	0.07	1.60	3.7	3.8	3.1	0.48		0.7	99.5	0.35
MAT-34	Granodiorite	2.68	Stage IV	-3.2	0.8		-	0.37	0.04	0.19	0.05	0.20	0.07	67.4	0.99	13.4	5.0	0.06	1.04	2.5	3.8	3.3	0.39	79	1.3	99.6	0.27
MAT-24	Granite	2.68	Stage IV	-3.1	0.8	-3.20	1	0.39	0.04	0.30	0.05	0.28	0.07	73.7	0.47	13.0	2.0	0.03	0.55	1.4	3.4	4.4	0.19	21	0.4	99.8	0.33
								0.34	0.07	0.16	0.15	0.19	0.12														
Hybrid granitoids																											
MOL-02b	Granite	2.68	Stage IV	n.a.	-	-3.20	0.7	0.33	0.04	0.21	0.05	0.31	0.07	66.8	1.1	13.7	4.6	0.06	1.27	2.3	4.0	3.5	0.41	68	0.91	99.2	0.33
MOL-05c	Granite	2.68	Stage IV	-2.7	0.8	-2.60	0.8	0.30	0.04	0.11	0.05	0.15	0.07	72.6	0.70	12.9	3.3	0.06	0.52	1.7	3.7	3.4	0.16	70	0.18	99.6	0.22
MTL-31	Granite	2.68	Stage IV	-2.9	0.8		-	0.41	0.04	0.24	0.05	0.38	0.07	73.1	0.28	13.4	1.5	0.02	0.36	1.1	3.8	5.1	0.09		0.5	99.4	0.30
MTL-43	Granodiorite	2.68	Stage IV	-3.4	0.8	-2.60	1.3	0.42	0.04	0.18	0.05	0.28	0.07	64.7	1.3	13.6	5.5	0.09	1.8	3.9	4.1	2.9	0.53		0.68	99.8	0.37
MAS-22	Granite	2.68	Stage IV	-2.4	0.8		-	0.37	0.04	0.16	0.05	0.22	0.07	72.8	0.43	12.9	2.1	0.04	0.46	1.5	3.9	4.3	0.12	49	0.44	99.3	0.28
MAS-24	Leucoranite	2.68	Stage IV	-3.3	0.8		-	0.44	0.04	0.21	0.05	0.32	0.07	76.0	0.21	12.2	1.1	0.02	0.23	0.50	3.5	5.3	0.07	22	0.51	99.7	0.28